Iranian Journal of Science and Technology, Transactions of Civil Engineering (2023) 47:3345–3356
https://doi.org/10.1007/s40996-023-01123-9

RESEARCH PAPER

The Mechanical and Fracture Characteristics of Low Fiber Content Slurry-Infiltrated Fiber Concrete

Muhammed Gümüş[1] · Barış Bayrak[1] · Oğuzhan Çelebi[2] · Haluk Görkem Alcan[1] · Gökhan Kaplan[2] · Ali Öz[3] · Abdulkadir Cüneyt Aydın[2]

Received: 13 June 2022 / Accepted: 17 April 2023 / Published online: 12 May 2023

Abstract

It is well known that fiber additives provide concrete with significant ductility after the peak load depending on the fiber content. However, due to workability and balling effects, the maximum usage limit of steel fibers is about 3% by volume. To overcome these obstacles, a cement-based slurry is infiltrated into the vacancies between steel fibers, which is a special type of fiber-reinforced concrete named SIFCON. Although the flexural response of SIFCON has been studied well, fracture characteristics have not been dealt with in depth. In this work, three-point static tests were conducted on notched beams produced with SIFCON with steel fibers (i.e., 0, 2.5, and 5.0% by volume). Fracture formations from the beginning to the end of the experiment were traced with the digital image correlation method. Test results show that the crack mouth opening displacement (CMOD)-to-net vertical deflection ratio was constant for the fiber ratios of 2.5 and 5.0%. It was also revealed that steel fibers significantly improved the fracture energy but slightly changed the initial fracture toughness of SIFCON. Nonlinear sectional analysis was also performed using several tensile models for fiber-reinforced concrete. The numerical results indicated that the peak load in the experiment was best estimated by the RILEM TC162-TDF tension model.

Keywords SIFCON · Steel fiber · Flexural test · Digital image correlation · CMOD · Sectional analysis

List of Symbols

a	Initial notched depth
A	Area of remaining unnotched ligament
b	Specimen width
d_f	Fiber diameter
d	Effective depth of the specimen
E	Young's modulus of concrete
E_f	Young's modulus of fiber
F	Configuration correction factor
f_c	Concrete compressive strength
$F_{R,1}$	Residual stress at the CMOD of 0.5 mm
$F_{R,3}$	Residual stress at the CMOD of 2.5 mm
$F_{R,4}$	Residual stress at the CMOD of 3.5 mm
f_{ctm}	Axial tensile strength of concrete
$f_{ctm,fl}$	Flexural tensile strength of concrete
G_F	Fracture energy up to peak load
h	Specimen overall depth
K_h	Size factor
K_{IC}^{ini}	Initial stress intensity factor
l_f	Fiber length
m	Mass of the specimen between supports
S	Clear span between supports
V_f	Volume fraction of fiber
W_0	Area under load–net vertical deflection curve up to the peak load
δ	Net vertical deflection
δ_0	Peak load deflection
τ_d	Bond strength between fiber and surrounding concrete

✉ Muhammed Gümüş
muhammedgumus@kafkas.edu.tr

[1] Department of Civil Engineering, Kafkas University, Kars, Turkey

[2] Department of Civil Engineering, Atatürk University, Erzurum, Turkey

[3] Narman Vocational School, Atatürk University, Erzurum, Turkey

1 Introduction

Steel fibers have been applied for several decades to ameliorate the quasi-brittle nature of ordinary concrete. Fibers used up to a certain amount improve the mechanical characteristics of hardened concrete such as flexural and splitting

strength but not compressive strength (Baran et al. 2012). Ductility and toughness properties are also enhanced by the addition of dispersed steel fibers. The main reason behind these developments is that the fibers engage the newly formed tensile cracks by bridging them (Shah and Ribakov 2011). Hence, the residual stresses transferred between crack faces increase depending on the volume fraction of fibers used. However, the usage limit of steel fibers in ordinary concrete is about 2% by volume, and a greater amount causes some workability and heterogeneity issues due to the balling effect (Elnono et al. 2009).

To take advantage of involving a high amount of steel fibers in the mechanical aspect, therefore, slurry-infiltrated fiber concrete (SIFCON) was invented by Lankard and Newell (1984). SIFCON is a special type of conventional fiber-reinforced concrete (FRC) but differs from FRC with respect to fiber amount utilized and manufacturing process. In SIFCON, the volume fraction of steel fibers varies between 6 and 30 vol%, which is very high compared to conventional FRC (Rao and Ramana 2005). SIFCON is produced by pouring flowable slurry into molds in which steel fibers are spread before casting. Considerable attention is paid to avoiding segregation while obtaining viscous and flowable concrete. Therefore, it is preferred that the maximum grain size of aggregates or other powder is usually less than 0.6 mm (Sonebi et al. 2005). A densified matrix phase and increased fiber content in composite material provide superior mechanical properties such as strength and toughness (Farnam et al. 2010). Thus, several experimental studies have been conducted to analyze the flexural behavior of SIFCON (Li et al. 2020; Aygörmez et al. 2020; Alcan and Bingöl 2019; Kim et al. 2018; İpek 2018; Canbaz and Ünüvar 2016; Beglarigale et al. 2016; Ipek et al. 2015, 2014; Yazıcı et al. 2006; Yan et al. 2002).

Li et al. (2020) reported that the flexural properties and fiber efficiency of functionally graded composite beams in which SIFCON was located at the bottom layer were greatly improved. Usage of 30-mm hooked-end steel fibers increased the peak load and toughness of the plain specimen by 3.3 and 48.8 times, respectively. Alcan and Bingöl (2019) compared the effect of steel and woolen polypropylene fibers on the bending response of SIFCON and found that steel fibers give the best results. Kim et al. (2018) stated that flexural strength and toughness vary proportionally with the steel fiber content in SIFCON. Ipek (2018) studied basalt aggregates in SIFCON as a substitutive material to quartz sand and concluded that flexural strength was almost irrespective of the aggregate type. Beglarigale et al. (2016) noted that while the high-temperature exposure up to 300 °C advances the flexure strength, further rise in the temperature results in detrimental effects. The effect of presetting pressure on the hardened mechanical properties of functionally graded concrete (Ipek et al. 2015) and only SIFCON (Ipek et al. 2014) were investigated experimentally. According to their experimental results, it was noted that both the flexural strength and the toughness were enhanced due to presetting pressures applied. Yazıcı et al. (2006) pointed out that fly ash replacement with cement amends the flexural strength, and this enhancement is prominent at 10 vol% of steel fibers. Yan et al. (2002) introduced the term "fractal dimension" to assess SIFCON behavior quantitatively. Then they disclosed the significant relationship between the fractal dimension and fiber ratio.

On the other hand, due to the size effect phenomena and the long tail in the flexural response of FRC, the strength criterion may lead to misjudgment of the performance evaluation of materials used (Shi et al. 2020). Several studies reported in Xie et al. (2021) attempt to implement fracture mechanics to determine the fracture performance of FRC. Benson and Karihaloo (2005) and Benson et al. (2005) determined the matrix fracture toughness of fiber-reinforced cementitious composites. However, the production process of fiber-reinforced cementitious concrete preferred by the authors in Benson and Karihaloo (2005) and Benson et al. (2005) evidently differed from that of SIFCON in which the slurry is infiltrated into the dispersed fibers. Furthermore, there exist very limited experimental studies on the fracture properties of SIFCON. Few researchers have reported that the fracture energy of SIFCON with low fiber content increases with the increasing fiber content (Ipek and Aksu 2019; Sengul 2018), and it significantly relies on the fiber orientation (Yazıcı et al. 2010). However, other fracture parameters of SIFCON such as stress intensity factor, energy release rate, and effective crack length have not been established well.

The main objective of this work is to examine the fracture properties as well as the flexural response of SIFCON with low fiber content. The three-point flexural test was applied on notched beams produced with slurry-infiltrated concrete with and without steel fibers. The cracking response was traced by the two-dimensional digital image correlation method (2D-DIC). The effect of the steel fiber ratio on the crack length and width, flexural strength, fracture energy, and stress intensity factor is discussed. In addition to the experimental study, nonlinear sectional analysis was also performed with several tension models recommended for FRC. Finally, the numerical results were compared with the experiment in terms of peak load and corresponding toughness to determine the most accurate model capable of simulating SIFCON. It was found that steel fibers lead to a significant rise in the fracture energy but a slight variation in the initial fracture toughness of SIFCON.

Table 1 Composition and hardened strength of mixtures

Mixtures	Weight (kg) per m^3					Compressive strength (MPa)
	Cement	Powder	Superplasticizer	Water	Steel fiber	
SF0	800	925	20	360	–	45
SF2.5					195	91
SF5.0					390	91

Table 2 Physical and mechanical properties of fibers

Diameter, d_f (mm)	Length, l_f (mm)	Density (kg/m^3)	Tensile strength (MPa)	Young's modulus, E_f (GPa)
0.55	35	7800	1345	200

2 Experimental Program

2.1 Materials and Mix Proportions

Table 1 summarizes the amount of ingredients for SIFCON used in this work. In order to obtain high concrete compressive strength, a high cement dosage was preferred in this study. The type of cement used was CEM I 52.5N Portland cement with a density of 3.15 g/cm^3. Marble powder with a maximum grain size of 600 µm was utilized as the filler. Coarse or fine aggregate was not used in this study with the aim of (i) achieving a densified matrix phase and (ii) decreasing segregation. High flowability of the slurry is desired for SIFCON due to its fiber content in large quantities. Therefore, a high water-to-cement ratio (w/c) of 0.45 was adopted for each mixture. Moreover, a polycarboxylate-based superplasticizer with a density of 1.07 kg/L was involved to satisfy the target consistency of the slurry. The amount of the superplasticizer used in each mixture was 2.5% of cement weight. The mixture name consists of the letters SF and the following number, which denotes the steel fiber and the volume fraction of steel fibers, respectively.

In this work, hooked-end steel fibers were employed for the manufacture of SIFCON. The amount of fibers used was 195 and 390 kg/m^3 which corresponds to the ratio of 2.5 and 5.0 vol%, respectively. The geometrical and mechanical features of the steel fibers used are given in Table 2.

2.2 Production of Specimens

A standard Hobart-type mixer with a 5 L capacity was operated to prepare the slurry of SIFCON. Cement and marble powder were first mixed in dry conditions for about 2 min at 140 rpm. Then, a liquid solution comprising water and superplasticizer was gradually added to the dry mixture and blended at 285 rpm for the next 5 min. Steel fibers were first placed into the steel mold as in Fig. 1a. Then the flowable slurry was poured into the steel molds. The casting of each specimen was completed in three layers to ensure sufficient homogeneity of the composite. Following the placement of each layer, one third of the steel fibers were evenly spread over the entire surface of the concrete layer. Finally,

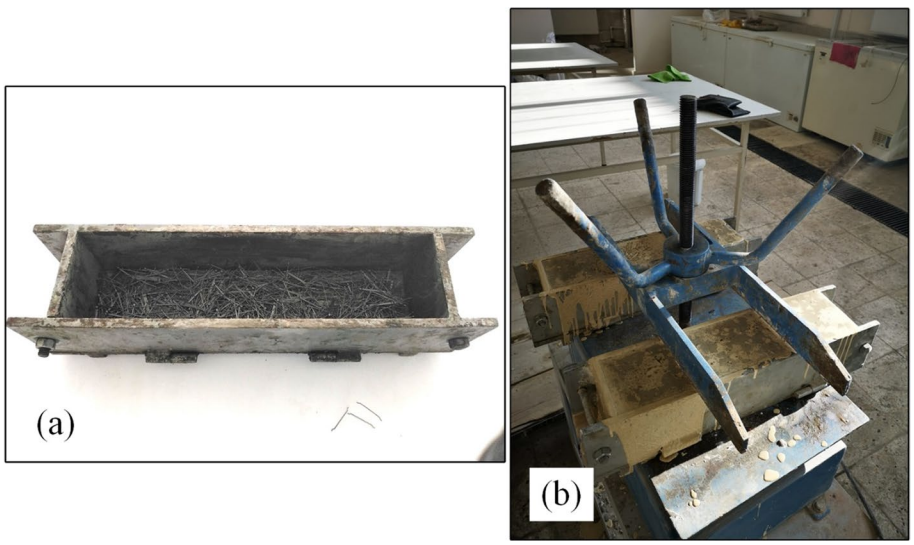

Fig. 1 Specimen production: **a** steel fibers in the mold and **b** infiltration of concrete slurry

to achieve better injection of slurry, fresh mixtures were compacted through a vibrating table, as seen in Fig. 1b. The surfaces of compacted SIFCON were covered with a plastic sheet to prevent moisture loss due to evaporation. At 24 h after casting, hardened concrete specimens were demolded and put into a water tank for about 7 days of water curing.

Cube specimens of $100 \times 100 \times 100$ mm and $100 \times 100 \times 400$ mm prisms were produced for compression and flexural tests, respectively. Three cubes and one prism sample were manufactured for each mixture specified in Table 1. Before the flexural tests, an edge notch perpendicular to the casting direction was opened at the center of the prisms using a circular saw. The length and width of the initial notch were 30 and 5 mm, respectively. Figure 2a illustrates the geometry of the notched beams with some relevant dimensions.

2.3 Setup and Measurements

Figure 2b shows the experimental test setup of notched beams. As is seen from the figure, three-point loading was adopted for testing of notched beams. A constant displacement loading of 0.1 mm/min was performed throughout the experiment by a hydraulic loading unit. The applied load was measured using a load cell mounted on the testing machine. Full-field deformations on the surface of the notched beams were obtained by implementing the 2D-DIC method. A Canon EOS 1300D digital camera and EF-S 18–55 mm lens were operated together. The digital camera had an 18 megapixel complementary metal–oxide–semiconductor (CMOS) sensor, which produces an image size of 5184×3456 pixels. The focal length of the lens used was set to about 50 mm to minimize distortions. The digital camera was fixed at a distance of about 1.5 m from the specimen so as not to cause incorrect measurements due to the vibration of the camera. Special attention was paid to aligning the lens and surface perpendicularly. Moreover, a remote control was used to release the shutter without physical touching, which would cause noisy data. During the testing of the notched beams, digital images were captured at time intervals of 5 s.

Prior to experiments on the notched specimens, specimen surfaces were properly prepared for measurement by image correlations. At first, the specimens' surfaces were polished by using a steel wire brush to clean up dust and other remnants. Then a white thin layer was created by using a lime solution on the surfaces to be analyzed. At the final stage, a random speckle pattern was formed over the white surface with black spray paint. Hence, the best contrast was obtained to be used for the correlation between the reference and deformed images. Furthermore, a light-emitting diode (LED) light was also employed to make evident the contrast between the black dots and the white background. Following the experiments, digital images were analyzed by means of an open-source algorithm by Blaber et al. (2015). Subset radius, subset spacing, and strain radius were taken as 33, 10, and 10 pixels, respectively. Concerning the location of the camera used in this work, the field of view was about 371×247 mm^2. This means that 1 pixel is associated with an approximate area of 72 μm squared or that the image resolution equals about 14 pixels/mm.

Net vertical deflections and crack mouth opening displacements (CMODs) were derived from the virtual points

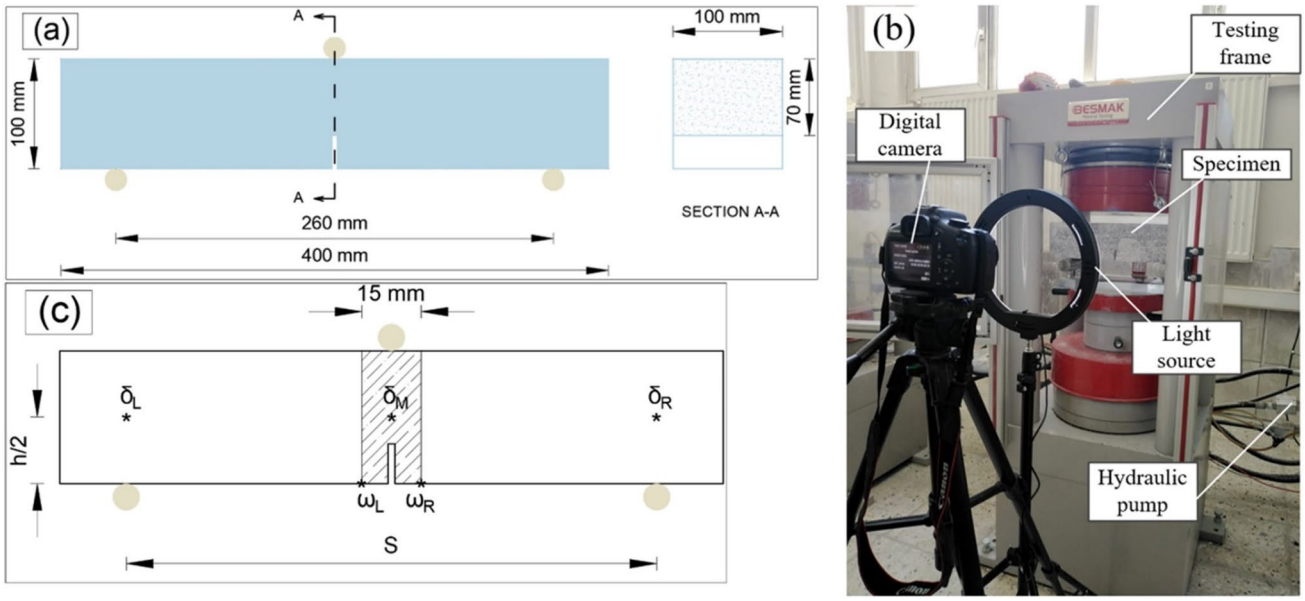

Fig. 2 Notched beam: **a** dimensions, **b** test setup, and **c** virtual points for measurements

located on the surface of the notched beams. Figure 2c displays the locations of those virtual points. Net vertical deflections were obtained such that the average of the supports' vertical deflections, $(\delta_L+\delta_R)/2$, were subtracted from the vertical deflections, δ_M, at mid-span. CMODs were computed as the absolute difference between the lateral deformations of ω_L and ω_R. In a similar way to the derivation of CMOD, crack opening displacement (COD) was also obtained from the multiple virtual points on the border of the shaded area in Fig. 2c. As is seen from Fig. 2c, the lateral distance between the virtual points of ω_L and ω_R was adjusted to 15 mm to capture the curvilinear shape of a cohesive crack occurring at a wide bandwidth.

3 Experimental Results and Discussions

3.1 Cracking Behavior of SIFCON

Figure 3 comparatively shows the crack patterns at the ultimate flexural loads obtained from the full-field lateral strain map. Limits of the contour bar for the strain levels vary according to the mixture for better visualization of the crack appearance. CMOD and crack length were also designated in the figure. It was observed from Fig. 3 that crack length and CMOD at peak load were significantly influenced by the amount of dispersed steel fibers. Critical CMODs of SF2.5 and SF5.0 mixtures reached 2.48 and 9.07 mm, respectively, compared to a CMOD value of only 0.02 mm for the SF0 mixture. Such impressive increments in CMODs resulted from the bridging effect of dispersed steel fibers. It is well known that steel fiber additives extend the tail of the load–deflection or load–CMOD curves. The reason is that steel fibers were activated when the major cracks localized after the ultimate load was reached (Soutsos et al. 2012). However, the test results of the present study indicate that the bridging phenomenon by steel fibers was activated even for the onset of the localization at the ultimate load.

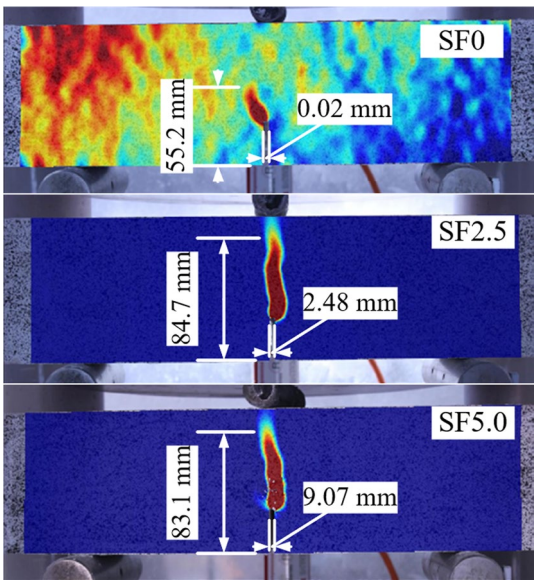

Fig. 3 Crack patterns at ultimate loads

It is also observed from the figure that the crack length of the SF2.5 mixture increased by 53% compared to that of the SF0 mixture. However, a further increase in the steel fiber content (5.0 vol%) caused a slight reduction of measured crack length by approximately 2% compared to that of the SF2.5 mixture. Such a decline could be attributed to the uneven distribution of steel fibers in the specimen geometry, which was promoted by the increase in fiber content. Hence, this heterogeneity triggered variation of the crack length from section to section along the specimen width. This finding correlates fairly well with the results in Chen et al. (1992) and Skarżyński and Tejchman (2016). Skarzynski and Tejchman (2016) analyzed the crack pattern of the notched beam by both X-ray micro-computed tomography (CT) and digital image correlation (DIC), and underlined the crack length variation along the specimen width.

3.2 Flexural Responses of SIFCON

In this section, the flexural responses of the notched beams produced with SIFCON were investigated in terms of load versus net deflection and load versus CMOD curves. Derivation of the net vertical deflection and CMOD from the experiments was explained in Sect. 2.3. Figure 4 compares the flexural behaviors of the notched beams, which were recorded until the significant drop in the load-bearing capacity appeared. It is observed from the figure that the overall load–vertical deflection shape highly resembles the companion load–CMOD curves. However, CMODs at an arbitrary load level in the descending branch were much greater than the corresponding net vertical deflections. As expected, this is a natural consequence of the bending test configuration.

Another significant inference from the test results is based on the cracking stiffness and post-peak slope on the load–deflection curves, because the obtained slope is an indicator of the mixture's brittleness. As observed from the magnified axes of load–vertical deflection, the cracking stiffness of the SF0 mixture between the cracking and peak load was identical to those of SF2.5 and SF5.0 mixtures. This shows that the initial cracking behaviors depend on the mechanical and physical properties of the matrix phase only. However, post-peak behaviors are considerably influenced by the presence of dispersed fibers. Consistent with this statement, the negative slope of the SF0 mixture after the peak load illustrated the brittleness of the reference mixture without fiber, while strain hardening behaviors of SF2.5 and SF5.0 mixtures exhibited ameliorated

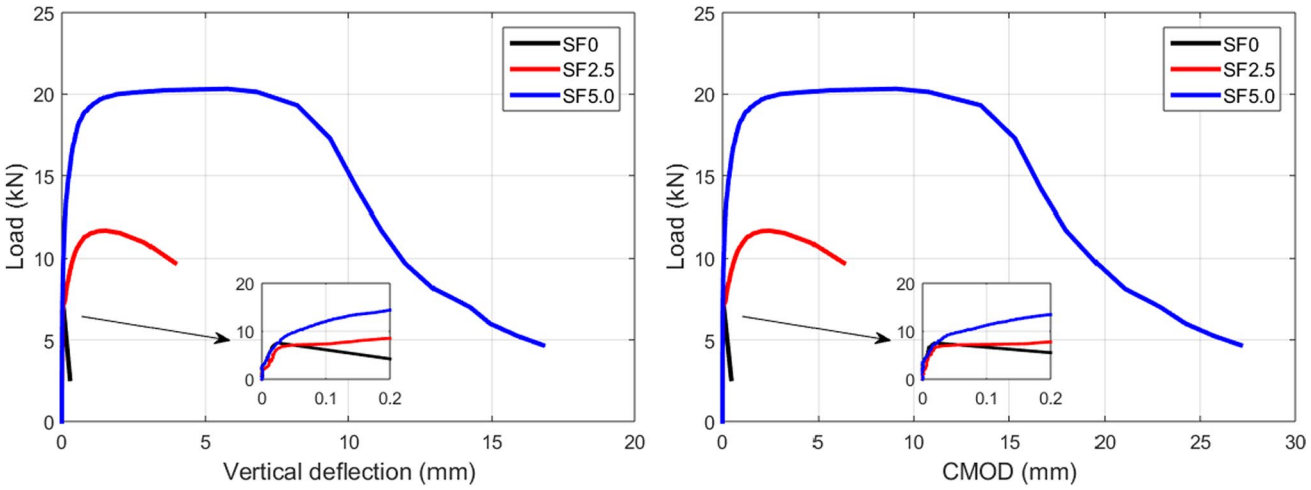

Fig. 4 Load–deflection and load–CMOD curves

Table 3 Experimental load and deflection values

Specimen	First cracking load (kN)	Peak load (kN)	Net vertical deflection (mm)	CMOD (mm)
SF0	2.94	7.58	0.02	0.02
SF2.5	2.17	11.69	1.55	2.48
SF5.0	2.92	20.33	5.75	9.07

load-bearing capacity due to steel fiber additive. Moreover, it should be noted that the volume fraction of dispersed steel fibers affected the post-peak slope of SIFCON. In the case of 2.5 vol% fiber usage, a gradual reduction in the load-bearing capacity was observed after the peak load. On the other hand, a wide yield plateau preceding the peak load was observed for the SF5.0 specimen, which shows improved ductility and energy-absorption capacity without unstable and rapid fracture.

First cracking and peak load, and vertical deflection and CMOD at peak load, are presented comparatively in Table 3, and their normalized values with the results from the SF0 mixture are drawn in Fig. 5. As seen from the load ratio in Fig. 5, the cracking load ratios of SIFCON marginally changed and fluctuated in the reference line irrespective of the vol% of the fibers. However, the peak load ratio proportionally increased with fiber additive. The load-bearing capacity of the SF2.5 and SF5.0 mixtures reached 1.54 fold and 2.68 fold of the SF0 mixture, respectively, due to the cohesive stress distribution along the crack plane given in Fig. 3. From the comparison of deflection ratios in Fig. 5, it is observed that both the vertical deflections and CMOD ratios of SIFCON obviously ascended as the fiber content in the SIFCON increased.

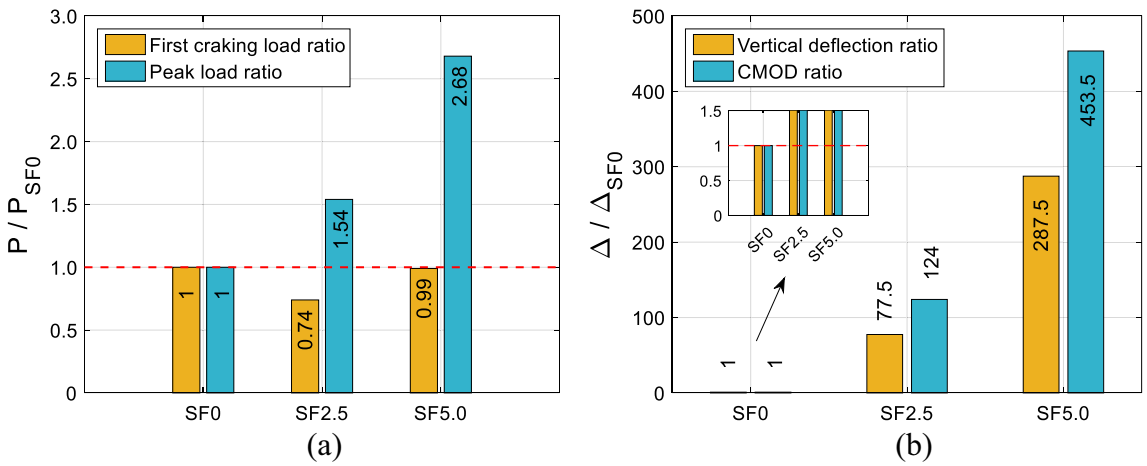

Fig. 5 Ratios of **a** measured load and **b** peak deformations to that of SF0

When the fibers were used at the ratio of 2.5 and 5.0 vol%, net vertical deflections were about 77 and 287 times larger than that of the mixture without fibers, respectively. Similarly, the CMODs of those mixtures were also increased by 123 fold and 453 fold compared to the plain mixture. Those results proved that the SICFON with steel fibers had a clear distinction in terms of deformation capacity and load-resisting level compared to the plain mixture.

It is also observed from Table 3 that the peak loads measured had a clear relationship with the corresponding net vertical deflections as well as the CMODs. As the peak load increased, both the net vertical deflection and CMOD increased almost linearly but in different proportions. The slopes of trendlines (best-fit equations) of the peak load (x-axis) versus deformations (y-axis) were approximately obtained as 0.46 and 0.72 for net vertical deflection and CMOD, respectively. On the other hand, the ratio of CMOD to net vertical deflection first increased from 1.0 to 1.6 when the steel fiber content was increased from zero to 2.5 vol%. However, it stayed constant at about 1.6 for the SF5.0 mixture irrespective of the further increase in the steel fiber content. According to the test results, it may be deduced that the variation of CMOD with net vertical deflection could be a material property for SIFCON with steel fibers. Those results agree well with the previous findings in Ding (2011). For the steel fiber-reinforced concrete, Ding (2011) reported that the relation between CMOD and vertical deflection could be assessed as a material property due to the high correlation between them.

Due to this evident relation, several experimental studies (Ding 2011; Almusallam et al. 2016; Aslani and Bastami 2015) and the design code (BS-EN 2005) recommended the equivalence defining the correlation between the net vertical deflection and CMOD of the notched concrete specimen with steel fibers. All the proposed equations are linear as in the following equation.

$$\delta = \alpha CMOD + \beta \tag{1}$$

where the notations of δ, α, and β represent the net vertical deflection and the coefficients of the linear equation. Table 4 demonstrates the equation's coefficients for different studies.

Figure 6 comparatively presents the ratios of the vertical deflections calculated by several methods to the companion measured values at peak loads. It is seen from the figure that all the empirical formulas overestimated the net vertical deflections from the experiments. The most conservative method was Aslani and Bastami's model which predicted the net vertical deflections of SF2.5 and SF5.0, respectively, by 1.53 and 1.41 times the measured ones. Contrary to that, net vertical deflections were best estimated with Almusallam et al.'s model such that the ratios

Table 4 Coefficients of the equations for different empirical models

Method	α	β
BS-EN14651 (2005)	0.8500	0.040
Ding (2011)	0.8830	–
Aslani and Bastami (2015)	0.8750	0.190
Almusallam et al. (2016)	0.7042	−0.121

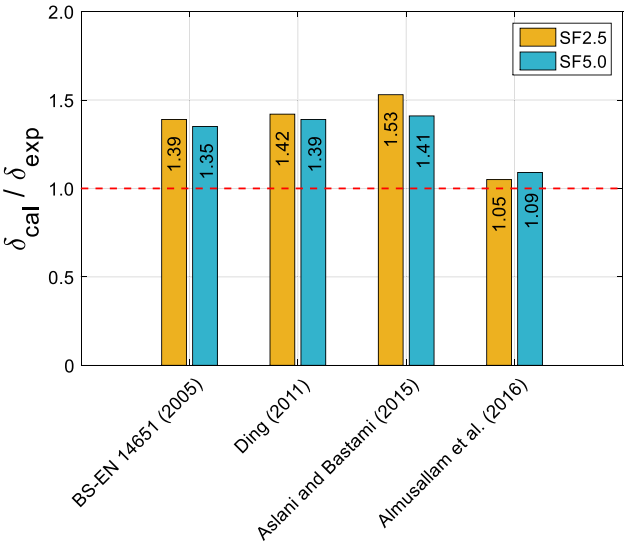

Fig. 6 Predicted-to-measured vertical deflection ratios

of predicted to observed net deflections were only 1.05 and 1.09 for the SF2.5 and SF5.0 mixtures, respectively. These dissimilarities in the predictions by different models may be caused by the span-to-overall depth ratios of notched specimens. According to the analytical derivation in the study by Ferreira (2007), a clear span between supports-to-depth ratio influences the net vertical deflection versus CMOD relation. This ratio was determined as 2.6, 3.0, and 3.33 for the present work, the model by Almusallam et al., and by Aslani and Bastami, respectively. Another observation from Fig. 6 is that the ratio of estimated to measured net deflection of the SF2.5 mixture was slightly larger than that of the SF5.0 mixture in all models except for Almusallam et al.'s model. Accordingly, it can be stated that the vol% of the dispersed steel fiber could be an effective parameter in determining the calculated-to-measured net vertical deformation ratio.

3.3 Fracture Parameters of SIFCON

Fracture energy is related to the work done by an external load applied to the specimen. It is one of the most practical characteristics of concrete fracture mechanics. Fracture energy can be obtained from the three-point bending test of a

notched specimen by integrating the area under the load–net vertical deflection curve up to a specific deflection which contains the ultimate deflection (RILEM-Recommendation-(TC50-FMC) 1985), peak load–deflection (Soroushian et al. 1998), a deflection level of 3 mm (Lee et al. 2018), and 3 times the peak load–deflection (Shi et al. 2020). In this work, peak load–deflection was preferred to evaluate the fracture energy (or energy release rate in this case) because none of the tests were continued to the deflection of complete fracture. Accordingly, fracture energy, G_F, at the peak load was computed for each mixture by implementing the following equation.

$$G_F = (W_0 + 9.81m\delta_0)/A \tag{2}$$

where W_0, m, δ_0, and A indicate the area under load–net vertical deflection curve up to the peak load, the mass of the specimen between supports, deflection at the peak load, and the area of remaining unnotched ligament, respectively.

Calculated fracture energies are plotted in Fig. 7. From the figure, it is seen that fracture energy raised from 0.02 to 2.32 N/mm and 16.01 N/mm, respectively, as the steel fiber content increased from zero to 2.5 and 5.0 vol%. This means that the fracture energy of the SF2.5 and SF5.0 mixtures reached 116 and 801 times that of the SF0 mixture, respectively. From the comparison of Figs. 7 and 5, it is seen that the most and the least contribution of fiber additives were on the fracture energy and peak load measured. In the case of 5.0 vol% fiber additive, fracture energy, CMOD, and peak load were increased by 800, 452.5, and 1.68 times the plain mixture without steel fibers, respectively. This result is consistent with the findings in Liu et al. (2022) and Magbool and Zeyad (2021). Magbool and Zeyad (2021) stated that the use of the steel fibers amended especially the post-peak region of the load–deflection curve, which resulted in a great

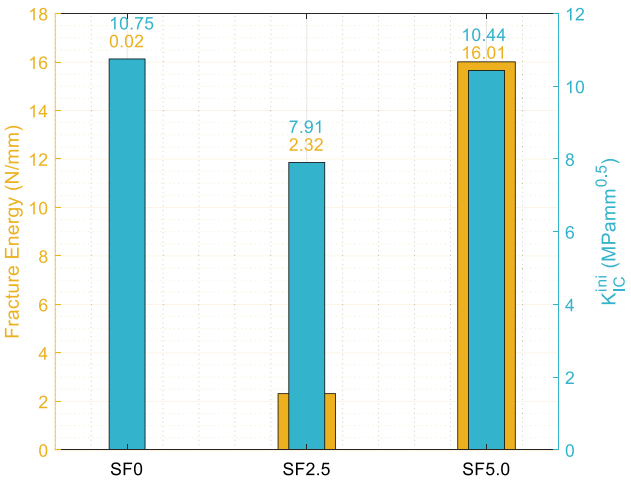

Fig. 7 Fracture energy and initial fracture toughness

improvement in the fracture energy by 22.8 times compared to the control mixture. In Liu et al. (2022), it was reported that steel fibers improved the load capacity by 103.1% but the fracture energy by 20.6 fold compared to the reference specimen at 28 days.

Fracture toughness is an indicator of the stress concentration at the tip of a cohesive crack. Thus, crack initiation could be evaluated in terms of initial fracture toughness, according to Xu and Reinhardt (2000). In this study, the initial fracture toughness (K_{IC}^{ini}) of SIFCON for the MOD-I test configuration was determined based on the following equation (Tada et al. 2000).

$$K_{IC} = \frac{1.5PS\sqrt{\pi a}F}{bh^2} \tag{3}$$

Here, P, S, and a symbolize the applied load, clear span between supports, and crack length, respectively. b and h stand for the width and depth of the specimen, respectively. F is a configuration correction factor that depends on the crack length, clear span, and overall depth of the specimen. For the span-to-depth ratio of 2.6, F is obtained by interpolation, as in Han et al. (2021). In the case of K_{IC}^{ini}, P and a equal the first cracking load and the initial notch length, respectively.

Predicted K_{IC}^{ini} values are given in Fig. 7 in comparison with fracture energy. As seen from the figure, the estimated K_{IC}^{ini} fluctuated as the fiber content increased. It decreased by about 26% when the fiber content was increased from 0 to 2.5 vol%. Contrarily, it increased by about 32% when the fiber content further increased from 2.5 to 5.0 vol%. According to the test results, it can be concluded that the effect of the steel fibers could be ignored in terms of the initial stress intensity factor of SIFCON. This inference could be confirmed by the findings in Liu et al. (2022), in which it was stated that the use of dispersed steel fibers indistinctly improves the initial fracture toughness of the shotcrete concrete.

4 Analytical Investigation of SIFCON

In this section, a nonlinear sectional analysis was conducted for SIFCON to find the best tension model simulating the flexural behavior of SIFCON. Therefore, a script was created to automatically perform sectional analysis based on the given tension and compression model. The moment versus curvature relation of the SIFCON was produced for the given specimen geometry and test configuration. Based on the elastic theory, the obtained theoretical responses were then converted to load versus net vertical deflection behavior. Figure 8 and Table 5 demonstrate the adopted tension models for steel fiber-reinforced concrete (Meng et al.

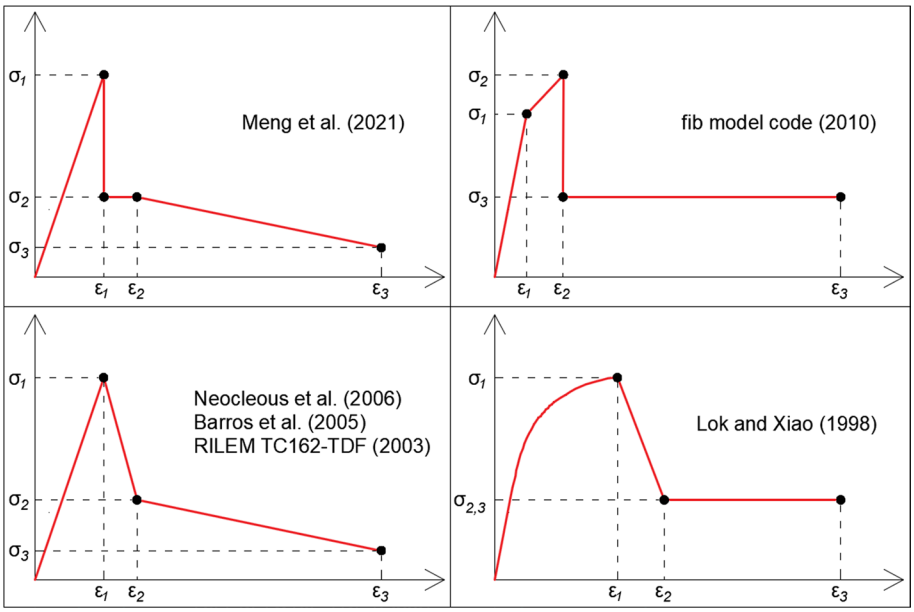

Fig. 8 Schematic view of the tension models

Table 5 Tension stress–strain laws according to the different models

	ε_1	ε_2	ε_3	σ_1	σ_2	σ_3
Meng et al. (2021)	σ_1/E	1.86‰	1.3%	$f_{ctm,fl}$	$0.39F_{R,1}$	$0.59F_{R,4}$–$0.26F_{R,1}$
Fib model code (2010)	σ_1/E	0.15‰	2.0%	$0.9f_{ctm}$	f_{ctm}	$0.33F_{R,3}$
Neocleous et al. (2006)	σ_1/E	$\sigma_2/E+2.0$‰	4.0%	$f_{ctm,fl}$	$f_{ctm,fl}e^{170(\varepsilon_1-0.002)}$	0
Barros et al. (2005)	σ_1/E	1.2‰	10.4%	$0.52f_{ctm,fl}(1.6-d)$	$0.36F_{R,1}K_h$	$0.27F_{R,4}K_h$
RILEM TC162-TDF (2003)	σ_1/E	$\varepsilon_1+0.1$‰	2.5%	$0.7f_{ctm,fl}(1.6-d)$	$0.45F_{R,1}K_h$	$0.37F_{R,4}K_h$
Lok and Xiao (1998)	$2\sigma_1/E$	$\tau_d(l_f/d_f)/E_f$	2.0%	f_{ctm}	$0.5V_f\,\tau_d\,(l_f/d_f)$	$0.5V_f\,\tau_d\,(l_f/d_f)$

2021; Fib Model Code 2010; Neocleous et al. 2006; Barros et al. 2005; RILEM-Recommendation-(TC162-TDF), 2003; Lok and Xiao 1998). It should be noted that the bond stress and axial tensile strength of concrete in Lok and Xiao's model were calculated as $\tau_d = 0.66f_c^{0.5}$ according to Campione (2008) and $f_{ctm} = 2.12\ln(1+(f_c+8)/10)$ according to Fib model code (2010), respectively. Effective depth, d, for the model by Barros et al. (2005) and RILEM-Recommendation-(TC162-TDF) (2003) was assumed to be equal to the remaining ligament length of 70 mm. Flexural tensile strength of concrete with fibers, $f_{ctm,fl}$, was predicted by using peak load up to the 0.05-mm CMOD value in accordance with BS-EN 2005. For the compression model, an elastic perfectly plastic stress–strain curve was adopted in this work. The ultimate compressive strain value was presumed as 0.0038 (Lok and Xiao 1998).

Figure 9 compares the theoretical and experimental load versus net vertical deflection response of SF2.5 and SF5.0 specimens. As can be seen from the figure, theoretical responses achieved by Lok and Xiao's model and Neocleous et al.'s model considerably diverged from the experimental response in the nonlinear region. This was probably a result of the adopted residual stress level in those models. For instance, the ultimate residual strength for the SF5.0 mixture was the highest in Lok and Xiao's model, 10 MPa, but the lowest in Neocleous et al.'s model, as shown in Table 5. It is also observed that the tail of the theoretical response obtained by Barros et al.'s model was the largest due to the ultimate strain capacity of 10.4% which was the highest one compared to that of others' models. Sudden drops in the theoretical load capacities estimated by Meng et al. (2021), Fib model code (2010), RILEM-Recommendation-(TC162-TDF) (2003), and Lok and Xiao (1998) were seen towards the end of the nonlinear regions. These were caused by relatively low ultimate strain capacity compared to that of Barros et al.'s model. As the tip of the main crack moved upwards from the initial notch, the most tension fiber of the specimen could not resist additional stresses due to the low ultimate tensile strain capacities of the models. Consequently, the reduced moment arm and the balancing lumped tensile force resulted in a rapid decrement in the load capacity of notched beams.

Further comparisons are based on the peak load and the toughness level from the load–deflection curve given in

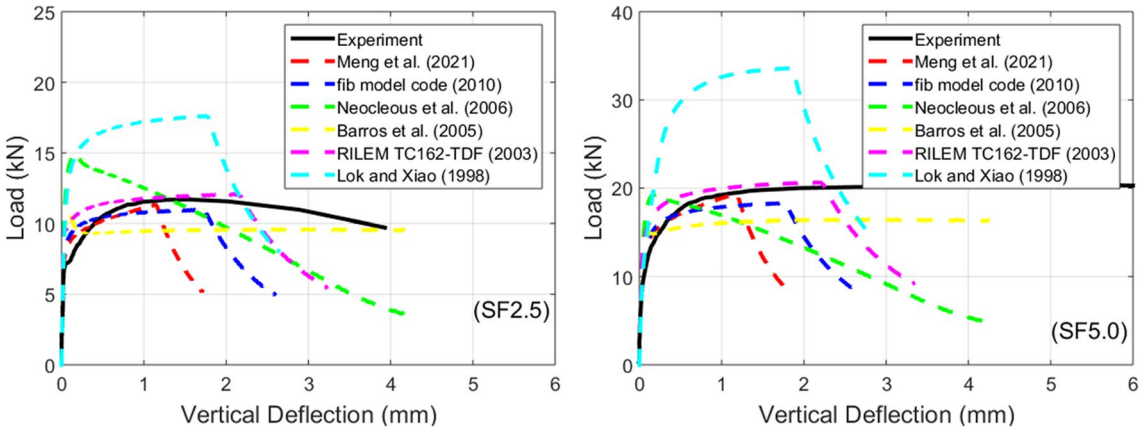

Fig. 9 Comparisons of the experimental and the numerical behaviors

Fig. 9. The theoretical peak load was normalized by that from the experiments. On the other hand, toughness was calculated as the area under the load–deflection curve up to the peak load for the theoretical response and normalized with the companion toughness from the experiment for the same deflection value. Obtained results are presented in Fig. 10 for both SF2.5 and SF5.0. Dashed lines in the figure signify the reference line which shows the equality of calculated and measured values. It is apparent from Fig. 10 that the most unsatisfactory model in simulating both the peak load and the accompanying toughness was Lok and Xiao's model. It yielded average errors of 58 and 66%, respectively, for the estimation of peak load and toughness. Contrarily, the numerical results proved that the peak load and the toughness were best predicted by RILEM TC162-TDF (2003) and Meng et al. (2021), respectively, with an average estimation difference of only 2.5 and 1.5%.

5 Conclusions

This research study focused on the effect of fiber content on the flexural characteristics of SIFCON. In this aspect, flexural responses and fracture parameters of SIFCON were examined by a three-point test setup for the edge notch beams. Following the experimental part of this work, a nonlinear sectional analysis was also performed using several tension models for steel fiber-reinforced concrete. According to the obtained experimental and numerical results, the main conclusions may be drawn as follows:

- Crack length at the peak load increased by 53% when the 2.5 vol% of fiber was used compared to the plain specimen. However, the rise of the fiber additive from 2.5 to 5.0 vol% led to an indistinct decline in the crack length by about 2%.
- The cracking stiffness of SIFCON with and without steel fiber was identical. However, post-peak responses of SIF-

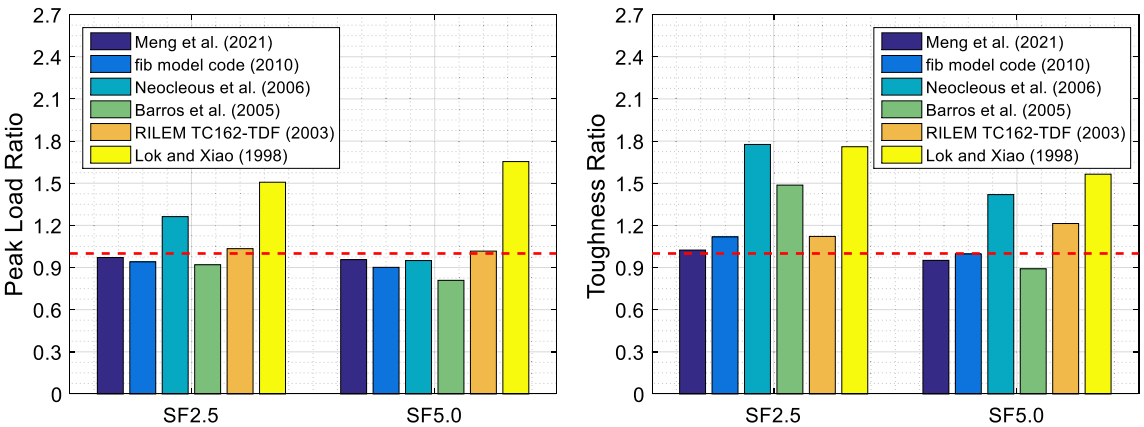

Fig. 10 Comparisons of normalized estimated peak loads and corresponding toughness

CON were substantially affected by the vol% of the steel fiber. Compared to the plain mixture, the bending capacity of the SIFCON with 2.5 and 5.0 vol% fiber ratios increased by 0.54 and 1.68 times. For SF2.5 and SF5.0 mixtures, those enhancement ratios were 76.5 and 277.5, respectively, regarding the net vertical deflection and 123 and 452.5 regarding the CMOD.

- CMOD to net vertical deflection at peak load were 1, 1.6, and 1.6 for the plain mixture, 2.5, and 5.0 vol% fiber ratios, respectively. It was found that this ratio was constant for the SIFCON with steel fibers and may be affected by the span-to-depth ratio of notched beams. Net vertical deflections of SF2.5 and SF5.0 were best estimated by Almusallam et al.'s model (2016) and worst estimated by Aslani and Bastami's model (2015). The average estimation differences in the Almusallam et al. and Aslani and Bastami models were 7 and 47%, respectively.
- For the fiber ratios of 2.5 and 5.0 vol%, the fracture energy of SIFCON up to the peak load reached 116 and 801 times that of the reference mixture without fiber, respectively. It is seen that the most and the least improvement due to fiber additive in SIFCON were on the fracture energy and peak load, respectively. An increase in the fiber ratio of SIFCON led to slight changes in K_{IC}^{ini}.
- Based on the nonlinear sectional analysis results, the simulation capability of the tension model for steel fiber-reinforced concrete by Lok and Xiao (1998) was the worst among the others considered. It resulted in an average difference of 58 and 66% regarding peak load and corresponding toughness, respectively. In contrast to that, peak load and toughness were best estimated with an average error of 2.5 and 1.5%, respectively, in the models by RILEM TC162-TDF (2003) and Meng et al. (2021).

Author Contributions MG: methodology, investigation, visualization, software, writing—original draft; BB: investigation, data curation, methodology; OÇ: methodology, investigation, resources; HGA: methodology, validation, visualization; GK: conceptualization, investigation, resources; AÖ: visualization, methodology; ACA: supervision, project administration, writing—review & editing.

Declarations

Conflict of interest The authors declare that they have no known competing financial interests or personal relationships that could have appeared to influence the work reported in this paper.

References

Alcan HG, Bingöl AF (2019) Examining SIFCON's mechanical behaviors according to different fiber and matrix phase. Iran J Sci Technol Trans Civ Eng 43(3):501–507. https://doi.org/10.1007/s40996-018-00227-x

Almusallam T, Ibrahim SM, Al-Salloum Y, Abadel A, Abbas H (2016) Analytical and experimental investigations on the fracture behavior of hybrid fiber reinforced concrete. Cem Concr Compos 74:201–217. https://doi.org/10.1016/j.cemconcomp.2016.10.002

Aslani F, Bastami M (2015) Relationship between deflection and crack mouth opening displacement of self-compacting concrete beams with and without fibers. Mech Adv Mater Struct 22(11):956–967. https://doi.org/10.1080/15376494.2014.906689

Aygörmez Y, Al-mashhadani MM, Canpolat O (2020) High-temperature effects on white cement-based slurry infiltrated fiber concrete with metakaolin and fly ash additive. Rev Constr 19(2):324–333. https://doi.org/10.7764/RDLC.19.2.324

Baran E, Akis T, Yesilmen S (2012) Pull-out behavior of prestressing strands in steel fiber reinforced concrete. Constr Build Mater 28(1):362–371. https://doi.org/10.1016/j.conbuildmat.2011.08.040

Barros JAO, Cunha VMCF, Ribeiro AF, Antunes JAB (2005) Post-cracking behaviour of steel fibre reinforced concrete. Mater Struct 38(1):47–56. https://doi.org/10.1007/BF02480574

Beglarigale A, Yalçınkaya Ç, Yiğiter H, Yazıcı H (2016) Flexural performance of SIFCON composites subjected to high temperature. Constr Build Mater 104:99–108. https://doi.org/10.1016/j.conbuildmat.2015.12.034

Benson SDP, Karihaloo BL (2005) Cardifrc®—development and mechanical properties. Part I: development and workability. Mag Concr Res 57(6):347–352. https://doi.org/10.1680/macr.2005.57.6.347

Benson SDP, Nicolaides D, Karihaloo BL (2005) Cardifrc®—development and mechanical properties. Part II: fibre distribution. Mag Concr Res 57(7):421–432. https://doi.org/10.1680/macr.2005.57.7.421

Blaber J, Adair B, Antoniou A (2015) Ncorr: open-source 2d digital image correlation matlab software. Exp Mech 55(6):1105–1122. https://doi.org/10.1007/s11340-015-0009-1

BS-EN 14651 (2005) Test method for metallic fibre concrete-measuring the flexural tensile strength (limit of proportionality (lop), residual), European Committee for Standardization

Campione G (2008) Simplified flexural response of steel fiber-reinforced concrete beams. J Mater Civ Eng 20(4):283–293. https://doi.org/10.1061/(ASCE)0899-1561(2008)20:4(283)

Canbaz M, Ünüvar C (2016) Effect of fiber and cement type on SIFCON properties. Pamukkale Univ J Eng Sci 22(6):400–404. https://doi.org/10.5505/pajes.2015.94547

Chen H, Cheng C, Chen S (1992) Determination of fracture parameters of mortar and concrete beams by using acoustic emission. Mater Eval 50(7):888–894

Ding Y (2011) Investigations into the relationship between deflection and crack mouth opening displacement of sfrc beam. Constr Build Mater 25(5):2432–2440. https://doi.org/10.1016/j.conbuildmat.2010.11.055

Elnono MA, Salem HM, Farahat AM, Elzanaty AH (2009) Use of slurry infiltrated fiber concrete in reinforced concrete corner connections subjected to opening moments. J Adv Concr Technol 7(1):51–59. https://doi.org/10.3151/jact.7.51

Farnam Y, Moosavi M, Shekarchi M, Babanajad SK, Bagherzadeh A (2010) Behaviour of slurry infiltrated fibre concrete (SIFCON) under triaxial compression. Cem Concr Res 40(11):1571–1581. https://doi.org/10.1016/j.cemconres.2010.06.009

Ferreira LET (2007) Fracture analysis of a high-strength concrete and a high-strength steel-fiber-reinforced concrete. Mech Compos Mater 43(5):479–486. https://doi.org/10.1007/s11029-007-0045-8

Fib Model Code 2010 (2010) First complete draft, volume 1, International Federation for Structural Concrete. https://doi.org/10.35789/fib.BULL.0055

Han X, Chen Y, Xiao Q, Cui K, Chen Q, Li C, Qiu Z (2021) Determination of concrete strength and toughness from notched 3 pb

specimens of same depth but various span-depth ratios. Eng Fract Mech 245:107589. https://doi.org/10.1016/j.engfracmech.2021.107589

Ipek M, Aksu M (2019) The effect of different types of fiber on flexure strength and fracture toughness in SIFCON. Constr Build Mater 214:207–218. https://doi.org/10.1016/j.conbuildmat.2019.04.055

Ipek M, Aksu M, Yilmaz K, Uysal M (2014) The effect of pre-setting pressure on the flexural strength and fracture toughness of SIFCON during the setting phase. Constr Build Mater 66:515–521. https://doi.org/10.1016/j.conbuildmat.2014.04.107

Ipek M, Aksu M, Uysal M, Yilmaz K, Vural I (2015) Effect of pre-setting pressure applied flexure strength and fracture toughness of new SIFCON+RPC composite during setting phase. Constr Build Mater 79:90–96. https://doi.org/10.1016/j.conbuildmat.2015.01.023

İpek M (2018) Examination of the usability of basalt aggregate in SIFCON. Civ Eng J Staveb Obz 27(4):500–512. https://doi.org/10.14311/CEJ.2018.04.0040

Kim S, Jung H, Kim Y, Park C (2018) Effect of steel fiber volume fraction and aspect ratio type on the mechanical properties of SIFCON-based hpfrcc. Struct Eng Mech 65(2):163–171. https://doi.org/10.12989/sem.2018.65.2.163

Lankard DR, Newell JK (1984) Preparation of highly reinforced steel fiber reinforced concrete composites. Spec Publ 81:287–306. https://doi.org/10.14359/6456

Lee SJ, Hong Y, Eom AH, Won JP (2018) Effect of steel fibres on fracture parameters of cementitious composites. Compos Struct 204:658–663. https://doi.org/10.1016/j.compstruct.2018.08.002

Li PP, Sluijsmans MJC, Brouwers HJH, Yu QL (2020) Functionally graded ultra-high performance cementitious composite with enhanced impact properties. Compos Part B Eng 183:107680. https://doi.org/10.1016/j.compositesb.2019.107680

Liu P, Guo C, Cui S, Wu Q, Xia W (2022) Fracture performance improvement and fracture process simulation of concrete for shotcrete use in hot and dry environments. Fatigue Fract Eng Mater Struct 45(5):1317–1331. https://doi.org/10.1111/ffe.13662

Lok TS, Xiao JR (1998) Tensile behaviour and moment–curvature relationship of steel fibre reinforced concrete. Mag Concr Res 50(4):359–368. https://doi.org/10.1680/macr.1998.50.4.359

Magbool HM, Zeyad AM (2021) The effect of various steel fibers and volcanic pumice powder on fracture characteristics of self-compacting concrete. Constr Build Mater 312:125444. https://doi.org/10.1016/j.conbuildmat.2021.125444

Meng G, Wu B, Xu S, Huang J (2021) Modelling and experimental validation of flexural tensile properties of steel fiber reinforced concrete. Constr Build Mater 273:121974. https://doi.org/10.1016/j.conbuildmat.2020.121974

Neocleous K, Tlemat H, Pilakoutas K (2006) Design issues for concrete reinforced with steel fibers, including fibers recovered from used tires. J Mater Civ Eng 18(5):677–685. https://doi.org/10.1061/(ASCE)0899-1561(2006)18:5(677)

Rao HS, Ramana N (2005) Behaviour of slurry infiltrated fibrous concrete (SIFCON) simply supported two-way slabs in flexure. Indian J Eng Mater Sci 12:427–433

RILEM-Recommendation-(TC162-TDF) (2003) Test and design methods for steel fibre reinforced concrete sigma-epsilon-design method. Mater Struct 36(262):560–567

RILEM-Recommendation-(TC50-FMC) (1985) Determination of the fracture energy of mortar and concrete by means of three-point bend tests on notched beams. Mater Struct 18(4):287–290

Sengul O (2018) Mechanical properties of slurry infiltrated fiber concrete produced with waste steel fibers. Constr Build Mater 186:1082–1091. https://doi.org/10.1016/j.conbuildmat.2018.08.042

Shah AA, Ribakov Y (2011) Recent trends in steel fibered high-strength concrete. Mater Des 32(8):4122–4151. https://doi.org/10.1016/j.matdes.2011.03.030

Shi X, Brescia Norambuena L, Tavares C, Grasley Z (2020) Semi-circular bending fracture test to evaluate fracture properties and ductility of cement mortar reinforced by scrap tire recycled steel fiber. Eng Fract Mech 236:107228

Skarżyński Ł, Tejchman J (2016) Experimental investigations of fracture process in concrete by means of x-ray micro-computed tomography. Strain 52(1):26–45. https://doi.org/10.1111/str.12168

Sonebi M, Svermova L, Bartos PJM (2005) Statistical modelling of cement slurries for self-compacting SIFCON containing silica fume. Mater Struct 38(1):79–86. https://doi.org/10.1007/BF02480578

Soroushian P, Elyamany H, Tlili A, Ostowari K (1998) Mixed-mode fracture properties of concrete reinforced with low volume fractions of steel and polypropylene fibers. Cem Concr Compos 20(1):67–78. https://doi.org/10.1016/S0958-9465(97)87390-8

Soutsos MN, Le TT, Lampropoulos AP (2012) Flexural performance of fibre reinforced concrete made with steel and synthetic fibres. Constr Build Mater 36:704–710. https://doi.org/10.1016/j.conbuildmat.2012.06.042

Tada H, Paris P, Irwin G (2000) The analysis of cracks handbook, 3rd edn. ASME Press, New York

Xie C, Cao M, Khan M, Yin H, Guan J (2021) Review on different testing methods and factors affecting fracture properties of fiber reinforced cementitious composites. Constr Build Mater 273:121766. https://doi.org/10.1016/j.conbuildmat.2020.121766

Xu S, Reinhardt HW (2000) A simplified method for determining double-k fracture parameters for three-point bending tests. Int J Fract 104(2):181–209. https://doi.org/10.1023/A:1007676716549

Yan A, Wu K, Zhang X (2002) A quantitative study on the surface crack pattern of concrete with high content of steel fiber. Cem Concr Res 32(9):1371–1375. https://doi.org/10.1016/S0008-8846(02)00788-3

Yazıcı H, Yiğiter H, Aydın S, Baradan B (2006) Autoclaved SIFCON with high volume class c fly ash binder phase. Cem Concr Res 36(3):481–486. https://doi.org/10.1016/j.cemconres.2005.10.002

Yazıcı H, Aydın S, Yiğiter H, Yardımcı Mert Y, Alptuna G (2010) Improvement on SIFCON performance by fiber orientation and high-volume mineral admixtures. J Mater Civ Eng 22(11):1093–1101. https://doi.org/10.1061/(ASCE)MT.1943-5533.0000114